Mechanical Systems and Signal Processing 50-51 (2015) 11–26

Contents lists available at ScienceDirect

Mechanical Systems and Signal Processing

journal homepage: www.elsevier.com/locate/ymssp

A case study to quantify prediction bounds caused by model-form uncertainty of a portal frame

Kendra L. Van Buren [a,*], Thomas M. Hall [b], Lindsey M. Gonzales [c], François M. Hemez [d], Steven R. Anton [e]

[a] Los Alamos National Laboratory, NSEC, Mail Stop T001, Los Alamos, NM 87544, USA
[b] Atomic Weapons Establishment, Berkshire RG7 4PR, UK
[c] University of Illinois at Urbana-Champaign, Urbana, IL 61801, USA
[d] Los Alamos National Laboratory, XTD-IDA, Los Alamos, NM 87544, USA
[e] Tennessee Technological University, Cookeville, TN 38505, USA

ARTICLE INFO

Article history:
Received 30 October 2013
Received in revised form
2 April 2014
Accepted 2 May 2014
Available online 20 June 2014

Keywords:
Uncertainty quantification
Experimental uncertainty
Test-analysis correlation
Finite element modeling
Parametric study
Bounding calculations

ABSTRACT

Numerical simulations, irrespective of the discipline or application, are often plagued by arbitrary numerical and modeling choices. Arbitrary choices can originate from kinematic assumptions, for example the use of 1D beam, 2D shell, or 3D continuum elements, mesh discretization choices, boundary condition models, and the representation of contact and friction in the simulation. This work takes a step toward understanding the effect of arbitrary choices and model-form assumptions on the accuracy of numerical predictions. The application is the simulation of the first four resonant frequencies of a one-story aluminum portal frame structure under free–free boundary conditions. The main challenge of the portal frame structure resides in modeling the joint connections, for which different modeling assumptions are available. To study this model-form uncertainty, and compare it to other types of uncertainty, two finite element models are developed using solid elements, and with differing representations of the beam-to-column and column-to-base plate connections: (i) contact stiffness coefficients or (ii) tied nodes. Test-analysis correlation is performed to compare the lower and upper bounds of numerical predictions obtained from parametric studies of the joint modeling strategies to the range of experimentally obtained natural frequencies. The approach proposed is, first, to characterize the experimental variability of the joints by varying the bolt torque, method of bolt tightening, and the sequence in which the bolts are tightened. The second step is to convert what is learned from these experimental studies to models that "envelope" the range of observed bolt behavior. We show that this approach, that combines small-scale experiments, sensitivity analysis studies, and bounding-case models, successfully produces lower and upper bounds of resonant frequency predictions that match those measured experimentally on the frame structure. (*Approved for unlimited, public release, LA-UR-13–27561*).

1. Introduction

Computational modeling in physics and engineering has become accepted to study the behavior of complex phenomena, especially when experiments are hindered due to time, money or safety constraints. For example, numerical models offer

* Corresponding author. Tel.: +1 505 663 5373.
E-mail address: klvan@lanl.gov (K.L. Van Buren).

http://dx.doi.org/10.1016/j.ymssp.2014.05.001
0888-3270/

a cost-effective alternative to investigate parametric studies of structural damage due to the cost and safety implications associated with full-scale destructive testing [1]. Further, when pursuing new concepts for design, computational models are useful to replace the traditional design, build and test paradigm. Numerical models have become commonplace to study the behavior of a wide range of structures, such as buildings, bridges, automobiles and wind turbines, as demonstrated by their inclusion in design standards [2–4]. While useful, it is emphasized that numerical models are developed using assumptions and simplifications, thus only being able to provide an approximation of reality. For this reason, the prediction uncertainty from numerical simulations must be quantified in order for simulation predictions to be effective in replacing or supplementing full-scale experiments.

Unavoidable sources of uncertainty exist when developing numerical models, such as experimental, parametric, numerical, and model-form (or structural) uncertainties. Reproducible and reliable experimental data are needed for use in calibration and validation assessments. However, experimental uncertainty is unavoidable, and can originate from variability of the manufactured product from design specifications, deviation of material properties from coupon properties used to represent the material behavior, and unique stress loading behaviors in critical sections of the structure [5]. Numerical uncertainty originates from the level of mesh discretization that is utilized in the model (or truncation error), round-off errors, numerical ill-conditioning, poor-quality interpolations and the lack-of-convergence of numerical solvers. In the case of truncation error, which is usually the dominant contributor, methods have been developed to produce error bounds for the resulting solution [6]. To ensure that the effect of mesh size on model output is minimal, it is typical to perform a mesh convergence study to identify the level of resolution that has an acceptably small effect on model predictions [7]. Parametric uncertainty is also commonly encountered when developing numerical models. This uncertainty represents, for example, the variability or unknown values of coefficients of a material constitutive model, energy restitution coefficients, or those of a contact condition between two surfaces. One approach is to treat these parameters as stochastic variables, for which probability laws are defined to create ranges of allowable values [8]. To identify parameters that exercise the most influence on model output, it is useful to use a phenomenon identification and ranking table, which can contribute to efficient parametric studies that include only the most influential parameters [9].

The last source of uncertainty discussed here, model-form uncertainty, is arguably more ambiguous than the experimental, numerical, and parametric uncertainties. Thus, attempts to quantify and realize the effect of model-form uncertainty have been far less encountered. Model-form uncertainty originates from assumptions or simplifications of known, or unknown, phenomena that must be represented in the numerical simulation. Assumption-making enables model building; it limits, however, the ability of the model to replicate reality [10]. When developing a model, its structural form is typically chosen based on theoretical considerations, goodness-of-fit to small-scale experiments, expert judgment, and computing constraints. This selection of a model form mitigates the lack-of-knowledge about the “best” modeling strategy that should be implemented; however, its effect on predictions often remains unknown. Some of the modeling assumptions that influence simulation results in structural dynamics include, but are not limited to: using a 1D, 2D, or 3D representation to model a component of the structure; the method through which contact and boundary conditions are represented; and the method through which external forces are applied. Due to the need for reliable simulation predictions, it is crucial to better understand the effect of model-form uncertainty on predictions.

When pursuing model-form uncertainty in structural dynamics, one area suggested as a topic of significance is the characterization of structural joints and connections [11]. After a decade-long research effort regarding the dynamics of jointed structures at Sandia National Laboratories, a recommendation is that more has to be achieved in order to quantify model-form uncertainty and “*assess the cumulative uncertainty of all elements playing a role in prediction*” [12]. Although much research has been conducted to understand the extent to which different joint modeling approaches accurately predict a dynamic response, more has yet to be discovered about how assumptions used in the development of these models affect numerical predictions. This work does not attempt to answer these questions for an arbitrary joint model. Instead, we propose a methodology that combines small-scale physical experiments, sensitivity analysis and the development of bounding-case models, and apply it to a relatively simple portal frame structure with bolted connections. Our goal is to estimate lower and upper bounds of resonant frequency predictions that are as consistent as possible with the experimental variability. This work builds on previous studies, which have already accounted for experimental, parametric and numerical uncertainties. The novelty is to consider and quantify model-form uncertainty. This comprehensive treatment of uncertainty is useful to understand the limitations imposed by simplifications applied to numerical models, which matters greatly if numerical simulations are expected to replace or supplement full-scale experiments.

The remainder of the paper is organized as follows. Design specifications and experimental setup of the portal frame are introduced in Section 2. Section 3 discusses the use of modal impact testing to measure the first four resonant frequencies. Experiments are conducted to characterize the variability that arises by changing the bolt torque, method of bolt tightening, and the sequence in which the bolts are tightened. Statistical Analysis-of-Variance (ANOVA) determines the sources of experimental variability that most significantly change the measurements. The most significant sensitivities learned from ANOVA are then used to guide the development of numerical models. Section 4 discusses the development of two competing Finite Element (FE) models implemented with the commercial software Abaqus™. Section 5 discusses test-analysis correlation between experimental measurements and numerical simulations, whereby the goal is to determine if the FE models provide ranges of predictions that are consistent with the ranges of measurements. Doing so leads to a better understanding of which model-form assumptions most significantly influence the predictions. Conclusions and recommendations for future work are given in Section 6.

2. Design specifications and experimental setup

To better understand how various modeling assumptions can affect prediction accuracy, a combined experimental and numerical study is performed on the nominally symmetric portal frame structure illustrated in the left image of Fig. 1. The structure is a bolted assembly of two vertical columns and a top, horizontal beam; the three-component frame is bolted to a base plate. We are interested in predicting the vibration response and, more specifically, the first four resonant frequencies. Close-up images of the joints are shown in the middle and right images of Fig. 1.

Dimensions of the portal frame are given in units of millimeters in the left image of Fig. 2. The material properties of the steel and aluminum metals are given in Table 1. Because these steel and aluminum metals are generic, their properties are typical values obtained from open-source material libraries. Table 2 lists the weights of components of the portal frame; the table also identifies the accelerometers used for instrumentation. Note that, in Fig. 2, the depth into plane is 50.8 mm, with exception of the base plate, which is 152.4 mm. The thickness of the vertical columns and horizontal top beam are identical, measuring 9.525 mm. L-brackets create the joint connections for the beam-to-column and column-to-base plate connections, with thickness of 6.35 mm. The beam-to-column connection is created using two large bolts, 12.7 mm in diameter and 25.4 mm in length. The column-to-base plate connection is created using a large bolt, also with a 12.7 mm diameter and

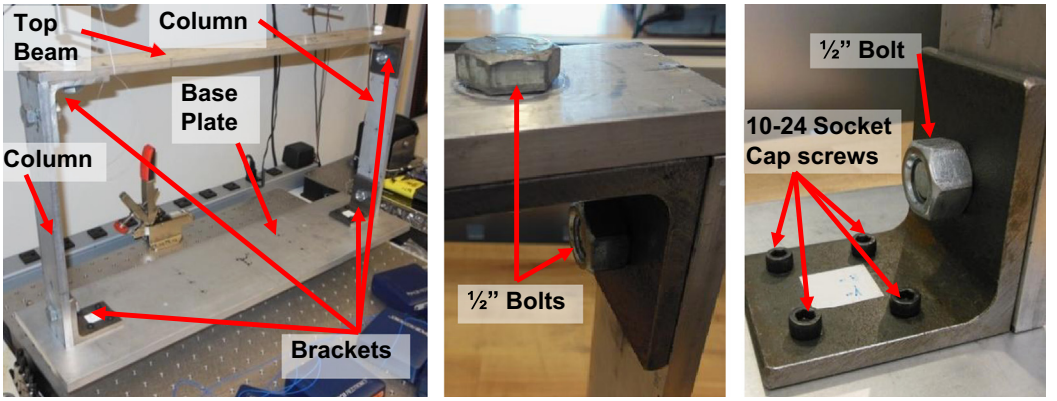

Fig. 1. Portal frame (left), top-side bolted joint (middle) and bottom of the frame (right).

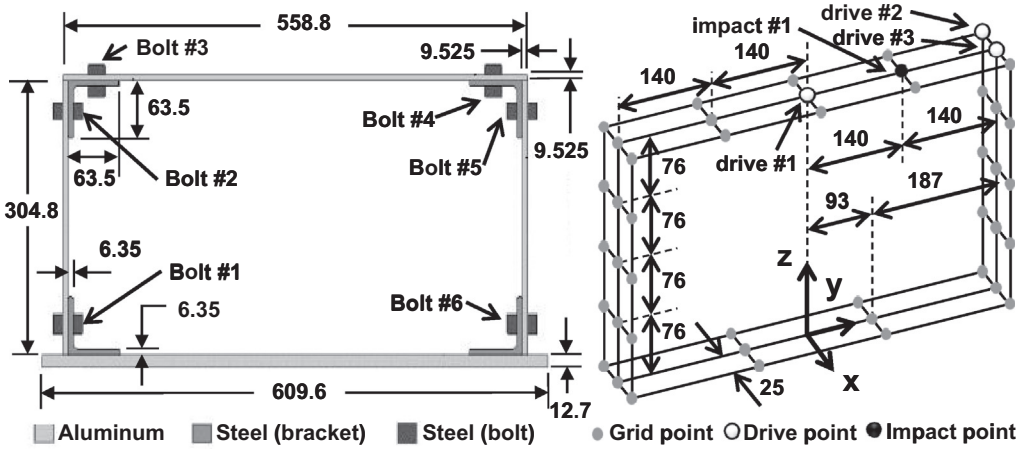

Fig. 2. Schematics of the portal frame structure with dimensions in mm.

Table 1
Material properties of the portal frame structure.

Material property	Steel	Aluminum
Young's Modulus, E (GPa)	200	69
Poisson's ratio, ν	0.29	0.33
Density, ρ (kg/m^3)	7861	2710
Shear modulus, G (GPa)	80	26

Table 2
Weight of individual components of the portal frame structure and experiments.

Component	Material	Weight (kg)
Top beam (horizontal)	Aluminum	0.720
Side column (vertical)	Aluminum	0.380
Base plate (horizontal)	Aluminum	3.160
Bracket (column-to-beam connection)	Steel	0.280
Bolt (column-to-beam connection)	Steel	0.038
Nut (column-to-beam connection)	Steel	0.016
10/24 Socket screw (column-to-base plate connection)	Steel	0.003
Uni-axial accelerometer (PCB piezotronics model 352C22)		0.0005
Tri-axial accelerometer (PCB piezotronics model 354C10)		0.0050

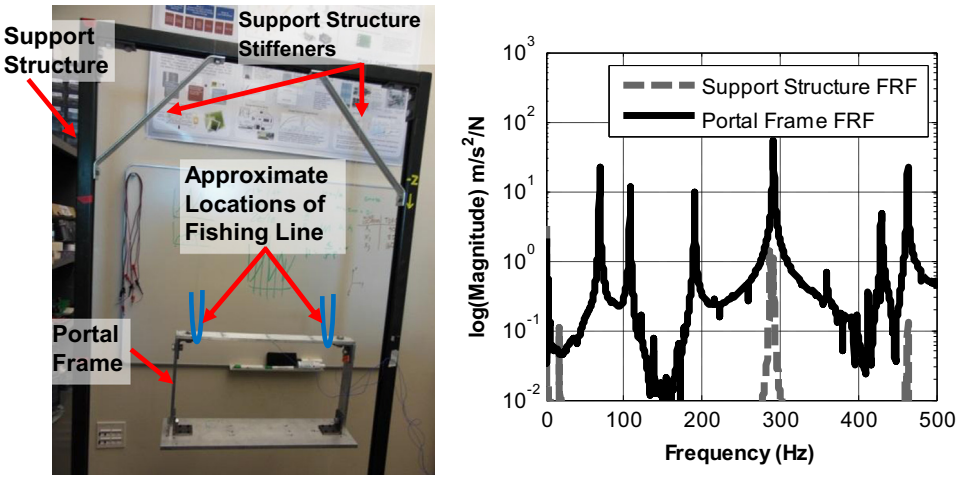

Fig. 3. Experimental configuration (left) and resonance peaks of the portal frame and support structure (right).

25.4 mm in length, to affix the column to the bracket, and four 10–24 socket cap screws, 12.7 mm in length, to connect the bracket to the base plate. For experimental testing, the bolts are numbered 1–6, starting from the bottom left bolt in Fig. 2 and moving clockwise around the structure.

The measurement points defined for experimental modal analysis are shown on the right side of Fig. 2. Measurement grid points are symmetric about the z-axis and y-axis as shown in the figure, where the z-axis intersects the mid-span of the top beam and base plate, and the y-axis is located along the centerline of the columns. For the vertical columns and top horizontal beam, measurement points are located at five equally spaced locations. For the base plate, measurement points are located at four equally spaced locations along the centerline and along two lines offset by 25 mm from the center. Fig. 2 also locates the three driving-point measurements on the top horizontal beam.

Although a somewhat simple structure, predicting with accuracy the dynamic response of the portal frame can be challenging. This challenge was recognized in previous studies, in which seven groups of three students at the 2008 Los Alamos Dynamics Summer School (LADSS) independently tested and modeled the structure [13]. A ± 3 standard deviation variability, which is denoted as $\pm 3\sigma$ in the remainder, of only 4 Hz was observed in the experiments, demonstrating the overall repeatability of modal testing, and $a \pm 3\sigma$ variability of 36 Hz was observed in numerical modeling. The main contribution to the prediction bias was attributed to the modeling of the boundary condition [13]. Herein, the boundary condition of the portal frame is better controlled, in both the experimental and numerical campaigns, than what was done during the 2008 LADSS study. For simplicity, especially on the modeling side, a free-free boundary condition is imposed.

The portal frame is suspended one meter from a support structure using fishing line as shown in the left image of Fig. 3; this approximates the free–free boundary condition. Based on pendulum equations as well as experimental data, the length of the suspension is deemed appropriate to ensure that the rigid body modes of the support structure are outside of the frequency range of interest. Stiffeners are added at the top corners of the support structure to suppress the coupling of its motion with that of the portal frame. To verify that the support structure provides a sufficiently rigid boundary condition, modal testing is performed by impacting the portal frame and measuring the response of both the portal frame and the support structure. The portal frame is instrumented with one tri-axial accelerometer located at the first drive-point, as shown in Fig. 2. The support structure is instrumented with two tri-axial accelerometers located on top of the frame where the fishing wire is attached to support the portal frame. Defining measurement locations that coincide with the fishing wire attachments enables the estimation of transmissibility of vibrations between the portal frame and support structure. Even

though a single measurement pair is shown on the right side of Fig. 3, impact hammer testing is replicated at multiple locations on the portal frame and it is verified that the results obtained remain consistent.

The right image of Fig. 3 compares the Frequency Response Functions (FRF) of the portal frame and support structure when the portal frame is impacted in the –z direction at the location labeled "impact #1" in Fig. 2. The portal frame data are shown with a black line; the support structure data are shown with a dashed gray line. These FRFs indicate that the fourth resonant frequency of the portal frame is around 200 Hz, whereas the first resonant frequency of the support structure is around 280 Hz. This observation confirms that the support structure is appropriate for experimental modal testing since coupling with the portal frame occurs outside the frequency range of interest. As noted previously, a similar conclusion is reached regardless of where the portal frame is impacted.

3. Experimental campaigns of vibration testing

Experimental testing explores the effect on measurements of varying control parameters of the frame structure. This exploration fulfills two objectives. The first one is to characterize the overall range of measurements, that is, the lower and upper bounds within which measured frequencies are expected to be observed for a similar structure. The second objective is to decompose this overall range of experimental variability to learn which control parameter, or combination of parameters, explains it. This understanding guides the development of numerical models.

The response features of interest are the first four resonant frequencies of vibration, which correspond to the shearing, torsion, out-of-bending, and in-bending modes. The mode shape deflections, illustrated in Fig. 4, are measured at the grid point locations defined in Fig. 2 using roving accelerometer testing. These vibration tests are carried out with a nylon hammer tip that excites within the bandwidth of 0-to-10^{+3} Hz, approximately, before the input force level drops more than 3 dB. A sampling rate of $2\times10^{+3}$ Hz is used and the response is measured at $2^{12}=4096$ samples. The modal assurance criterion is used to confirm that the experimentally observed mode shapes match the order of those obtained numerically. Relevant information of the experimental campaign is summarized here such that the discussion is self-contained as much as possible. Further details, including the pre-test verification checks of experimental assumptions and preliminary vibration testing results, can be found in Ref. [14].

Herein, testing is performed to explore the effect of varying the torque condition applied to the bolts. The measurements are collected with a sampling rate of 500 Hz, using a rubber impact hammer tip, and 8192 samples. Drive-point measurements are defined by impacting only at locations of accelerometers. Throughout the experimental campaign, three uni-axial accelerometers are located and maintained at the drive-point measurement positions, as shown previously in Fig. 2. Hammer impacts are applied in the –z direction at the first drive-point location, in the $+x$ direction at the second drive-point location, and in the –y direction at the third drive-point location. Ten replicates are carried out at each location to improve the signal-to-noise statistics through conventional processing steps (averaging, filtering, and windowing). It is verified that these experimental settings provide sufficient data quality; they are kept identical for all experimental campaigns to remain consistent as much as possible between the different measurements.

3.1. Effect on the measured response of varying the bolt torque level

The first study conducted is to determine how the bolt torque level affects the structural behavior of the portal frame. Torque is increased from 4.52 Nm to 9.04 Nm and 18.08 Nm. Impact hammer testing is repeated for each level of torque. The sequence in which the bolts are tightened remains the same for all tests performed, so as to not introduce additional variability to the experimental results. The tightening order used is 2–3–6–4–5–1 (recall the bolt numbering provided in Fig. 2). This sequence is chosen due to its somewhat star-like pattern, which is similar to approaches used to tighten bolts on a car tire in order to inhibit misalignment.

Table 3 reports the average values of resonant frequencies obtained at each torque level. The trend observed is unambiguous: as the torque is increased, the portal frame becomes stiffer and the resonant frequencies begin to rise. Fig. 5 displays a visual comparison of this trend by reporting the behavior of normalized frequency changes. The normalized changes are defined as deviations from the average frequency for each mode. The measurements of Table 3 are used to calculate the normalized frequencies for each mode. Table 3 and Fig. 5 indicate that the resonant frequencies of modes 1, 2 and 4 are affected by changes to the bolt torque level, while those of mode 3 remain nearly unchanged. A reason why modes

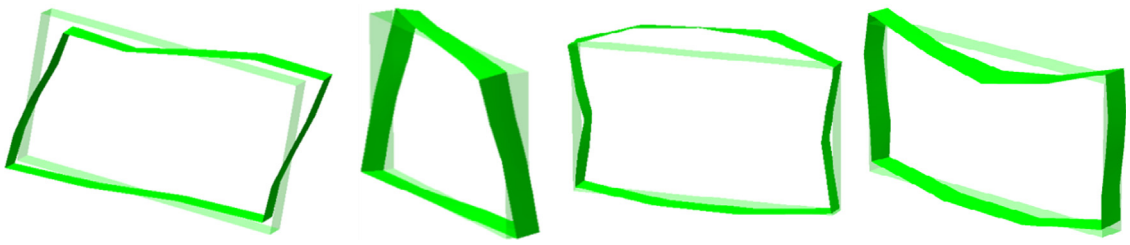

Fig. 4. First four resonant mode shapes identified from experimental testing.

Table 3
Resonant frequencies obtained by changing the bolt torque level.

Torque level (Nm)	Measured resonant frequency (Hz)			
	1st-Shearing	2nd-Torsion	3rd-Out-bending	4th-In-bending
4.52	58.9	97.6	104	172
9.04	62.8	101	104	178
18.08	67.9	102	105	186

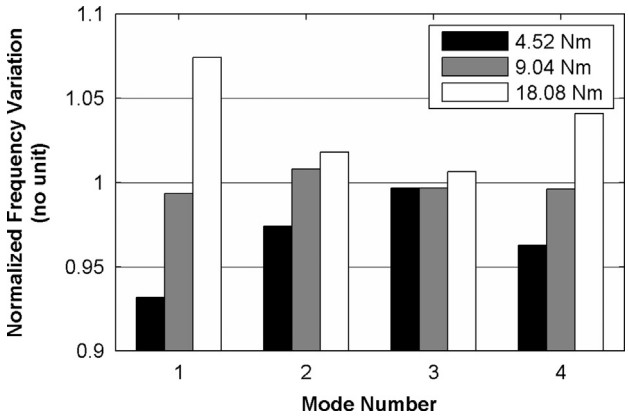

Fig. 5. Normalized frequencies obtained by changing the bolt torque level.

Table 4
Resonant frequencies obtained with two bolt-tightening procedures.

Torque level (Nm)	Tightening procedure	Measured resonant frequency (Hz.)			
		1st-Shearing	2nd-Torsion	3rd-Out-bending	4th-In-bending
4.52	Direct	58.9	97.6	104	172
	Gradual	58.8	97.6	103	172
9.04	Direct	62.8	101	104	178
	Gradual	63.9	100	104	179
18.08	Direct	67.9	102	105	186
	Gradual	68.1	102	105	186

1, 2 and 4 are more sensitive to the bolt torque level might be that their deflections involve significant shearing or frictional effects at the joints, as shown by the mode shape deflections in Fig. 4. As torque increases, so does the normal force being applied to the bracket and beam surfaces in contact with each other, and so does friction. Therefore, it makes sense that deformation modes involving shearing and friction would be more sensitive to changes in bolt torque, at least, in the low frequency range. The third mode, on the other hand, involves out-of-phase bending that might pull apart beams in contact in the direction normal to their surfaces. If so, then the third mode would be less sensitive to bolt torque while it is influenced, instead, by bolt material properties.

3.2. Effect on the measured response of changing how the bolt is torqued

Having developed an understanding of how bolt torque affects the modal frequency data, the method by which the bolts are tightened is considered next. The initial bolt torque study in Section 3.1 considered the behavior of the portal frame when the bolts are tightened directly to the specified values of torque used in the experiments. Here, additional testing is conducted to observe the extent to which gradually increasing the bolt torque provides a different level of experimental variability as opposed to directly increasing the bolt torque.

The torque levels are increased incrementally by steps of 1.13 Nm at each bolt location. The same sequence of bolt tightening (2–3–6–4–5–1) as the one used in the original study is used; it avoids biasing the comparison by introducing another factor in the analysis. The incremental tightening is performed to ensure that each bolt has a snug fit when tightened. When increasing, for example, the torque from 4.52 Nm to 9.04 Nm, each bolt is tightened to 5.65 Nm using the specified tightening sequence. Each torque is then increased to 6.78 Nm, then to 7.91 Nm and, finally, to 9.04 Nm.

A comparison of resonant frequencies is given in Table 4. There is now a total of six frequencies for each mode, from the combination of three bolt torque levels and two tightening procedures (direct vs. gradual) for each torque. Comparing the resonant frequencies as the torque level is increased leads to the same observation as before (Section 3.1). Applying more torque stiffens the structural joints and, consequently, resonant frequencies of the portal frame increase.

The second comparison is what happens when the tightening procedure is modified at a given level of bolt torque. Table 4 indicates that the resulting variation of resonant frequencies is, at most, 1 Hz. Gradually tightening the bolts, instead of directly applying the specified torque, sometimes increases a frequency and, other times, tends to reduce it. The conclusion is that the procedure of bolt tightening has little-to-no influence on the behavior of the structure.

3.3. *Effect on the measured response of changing the bolt tightening sequence*

The experiments discussed in the previous two sections used a constant sequence in which the bolts are tightened. Here, the effect that the tightening sequence has on experimental variability is investigated. The study considers five different sequences at each one of the three torque levels. Table 5 shows the five sequences considered, where the bolt numbers are as defined previously in Fig. 2. For each experiment performed in this study, the bolts are tightened from finger-tight directly to the torque level specified.

The bar graph in Fig. 6 shows the normalized frequencies obtained for the five tightening sequences at the 4.52 Nm torque level. There is no visible trend that would suggest that the bolt tightening sequence affects resonances of the portal frame in a systematic and consistent way. Furthermore, the changes observed remain small compared to those illustrated in Fig. 5, where the effect of bolt torque level is investigated.

Table 6 reports the ranges of resonant frequencies obtained when the bolt tightening sequence is varied. Most cases exhibit a few Hz of variability, up to 10 Hz in the case of the in-phase first bending mode (18.08-Nm torque level). It is clear

Table 5
Definition of tightening sequences.

Experiments 1–2		Experiments 3–4		Experiment 5	
Sequence	**Bolt order**	**Sequence**	**Bolt order**	**Sequence**	**Bolt order**
1	2–3–6–4–5–1	3	6–2–3–1–4–5	5	1–6–2–5–3–4
2	2–3–4–5–6–1	4	1–2–3–4–5–6		

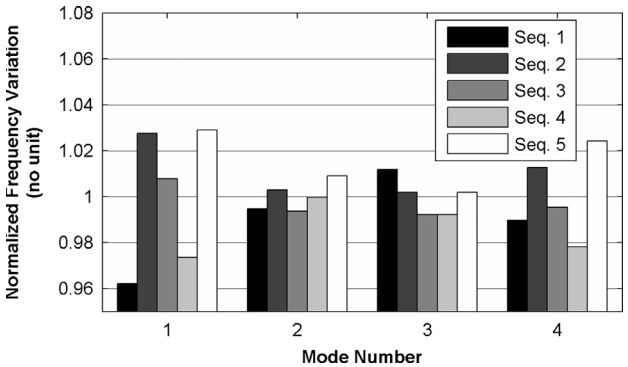

Fig. 6. Normalized frequencies obtained by changing the bolt tightening sequence at the 4.52 Nm torque level.

Table 6
Ranges of frequencies obtained by varying the bolt tightening sequence.

Torque level (Nm)	Measured resonant frequency (Hz)							
	1st-Shearing		2nd-Torsion		3rd-Out-bending		4th-In-bending	
	Low	**High**	**Low**	**High**	**Low**	**High**	**Low**	**High**
4.52	58.9	63.0	97.5	99.0	102	104	170	178
9.04	63.7	66.6	99.8	101	104	105	180	185
18.08	66.3	71.6	102.0	103	105	106	183	193

that the bolt tightening sequence provides greater experimental variablity than the procedure used to tighten the bolts (see Section 3.2).

Based on comparing Table 3 (effect of the bolt torque level), Table 4 (effect of the tightening procedure) and Table 6 (effect of the tightening sequence), it appears that the ranking of influences from most important to least important is: (1) bolt torque level, (2) tightening sequence and (3) tightening procedure. This finding is confirmed next using a statistical method of variance decomposition.

3.4. Overall assessment of experimental variability

An Analysis-of-Variance (ANOVA) is conducted next to confirm the observations made in Sections 3.1–3.3. The ANOVA is a statistical method that expresses the total variance of the measured frequencies of the portal frame, as a decomposition of partial variances [14].

Results of the main-effect ANOVA are given in Fig. 7. Statistics for the tightening procedure are omitted because the R^2 values are small compared to the others. For convenience, the R^2 values are normalized mode-by-mode to add to 100%. As postulated, the level of torque has the greatest influence on resonant frequencies of modes 2–4. Contributions to the variability of the first resonant frequency (shearing mode, shown in black) are shared almost equally between the bolt torque level and tightening sequence. This suggests that reaching a high level of test-analysis correlation might be more difficult for the shearing mode because the physical measurements are influenced by a factor that is more involved to simulate numerically. It is emphasized that these results are from a main-effect analysis. As such, they do not capture the influence on frequency variability of a potential interaction between two, or more, factors.

Results from the statistical analysis reaffirm the empirical observations of the previous three sections. Increasing the bolt torque increases the overall stiffness of the structure, which causes the resonant frequencies to increase as well. The sequence in which the bolts are tightened has minimal influence on resonant frequencies, except for the shearing mode.

To conclude the analysis of experimental campaigns, the overall ranges of measured resonant frequencies are reported in Table 7. These ranges are used in the following to assess the prediction accuracy of finite element models. The third, out-of-phase first bending, mode is least sensitive to the experimental conditions tested. The difference in variability observed for the first four resonant modes might be explained by the shearing "action" in the joints of mode shapes, where resonant frequencies with more variability correspond to deformation shapes with more shearing at the contact surfaces. Findings, such as this one, are useful to guide the development of numerical models.

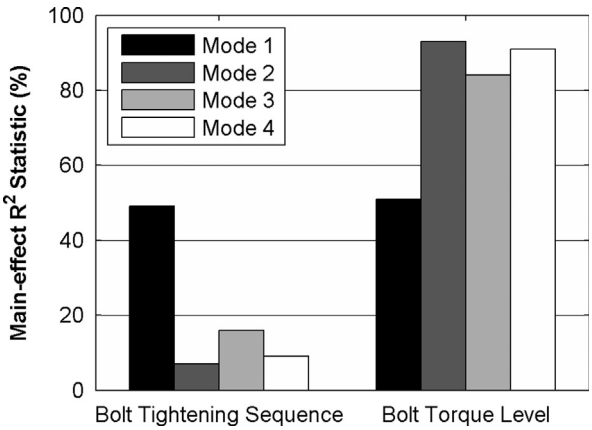

Fig. 7. Main-effect decomposition of measured resonant frequency variability.

Table 7
Overall ranges of resonant frequency variability (from measurements).

Torque level (Nm)	Measured resonant frequency (Hz)							
	1st-Shearing		2nd-Torsion		3rd-Out-bending		4th-In-bending	
	Low	High	Low	High	Low	High	Low	High
4.52	58.8	63.0	97.5	99.0	102	104	170	178
9.04	62.8	66.6	99.8	101	104	105	180	178
18.08	66.3	71.6	102.0	103	105	106	183	193

4. Finite element models of the portal frame

After assessing the experimental variability, and studying which factors are most influential to change the resonant frequency values, we proceed with the development and "validation" of numerical models. Model validation, here, has a particular meaning. The goal is not to demonstrate, through a combination of parameter study and calibration, that model predictions can reproduce the measurements. Instead, the objective is to develop numerical models whose predictions "envelope" the experimental variability assessed in Section 3.

To do so, two Finite Element (FE) models are developed using the modeling and analysis software Abaqus™ version 6.12. The models are used to study model-form uncertainty associated with the behavior of beam-to-column and column-to-base plate connections. All structural components (horizontal top beam, vertical columns, base plate, and attachment brackets) are modeled using three-dimensional, 8-noded solid elements. Ref. [15] gives a theoretical reference for the elements utilized. To simplify the model development, and make it easier to control the aspect ratio of elements, the rounded geometry of the brackets is ignored such that their corner angles are at 90°. This approximation is not detrimental to accuracy because the FE models are developed to capture the low-frequency dynamics, which are more strongly influenced by the overall distributions of stiffness and inertia properties than details of the geometry. Further details of the numerical modeling can be found in Ref. [14].

4.1. Development of the "bounding-case" finite element models

Instead of developing a single FE model whose predictions reproduce the measurements as best as possible, our goal is to assess the effect that competing model-form assumptions have on predictions. This goal is achieved by developing two FE models. The starting point is the three-dimensional geometry represented with solid elements mentioned above. Assumptions are then formulated to describe the behavior of beam-to-column and column-to-base plate connections.

From the experimental campaigns discussed previously, it is clear that the bracket connections allow for some degree of compliance at contact surfaces. This is evident from the influence exercised by procedures such as the tightening sequence. In the presence of an "infinitely rigid" interface that exhibits no compliance, there would be no mechanism for the tightening sequence to exercise any influence at all. On the other hand, we have observed that resonant frequency values are strongly influenced by the level of applied torque. It means that, even though the jointed connections might introduce some compliance, the contact condition is also sensitive to the normal preload applied by the bolts.

From these observations, the collection of models, which could be developed to represent the bracket behavior, can be defined along two dimensions. The first dimension is the degree of compliance of the joint and the second dimension is the region over which this compliance exercises an influence. In this study, a contact stiffness strategy is used to explore the compliance of the joint and a tied node representation is utilized to explore the region of action of the joint.

The contact stiffness representation of the frame uses three-dimensional translational spring elements at coincident nodes of the bracket-to-beam, column, or base plate connection. Spring coefficients are specified in the normal (k_{nn}) and two orthogonal shear (k_{ss} and k_{tt}) directions; these are used to parameterize the FE model for sensitivity analysis and calibration. Defining independent stiffness values in all three directions constrains translational motion of the joints, and thus, can constrain motion rotationally as well. For this reason, rotational springs are not considered to parameterize the FE model. Directions of the springs, with respect to orientation of the bolt, are specified in Fig. 8. It is emphasized that these coefficients are non-physical parameters and, therefore, unknown. In the tied node representation, nodes of the two surfaces in contact are tied together, which is a condition that does not allow for any relative displacement. The tied nodes are only active over a circular region of given radius, with the radius allowing parameterization of the FE model.

Other modeling strategies, for example, using solid elements to represent the bolts explicitly or imposing "fictitious" springs over a radius-of-influence, offer further alternatives. It is emphasized that the development of detailed, high-fidelity models of joint structural components has been an area of active research [16,17]. It would be possible to couple such high-fidelity models of the joints with our solid model of the frame components [18]. Herein, only the above two strategies are

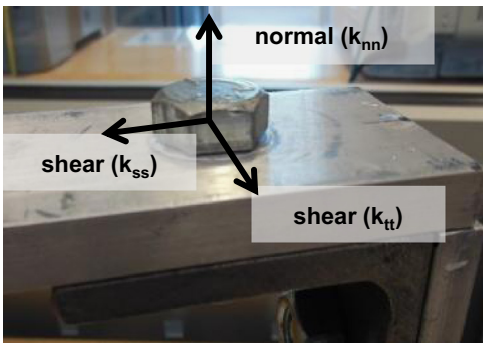

Fig. 8. Direction of "fictitious" springs in the contact stiffness model.

investigated because, first, they define bounding cases of how the jointed connections might behave and, second, they represent simplifications commonly encountered in the modeling and simulation community.

Each modeling strategy introduces its own parameterization. Unknown parameters of the two FE models are listed in Table 8. The spring stiffness coefficients and radius-of-influence are unknown because they are non-physical. For this reason, parametric studies are carried out to assess the behavior of the models as the values of their unknown parameters are varied. Parametric studies are performed using full-factorial designs of computer experiments. The choice of full-factorial designs offers advantages for sensitivity analysis in addition to a simple implementation.

By definition, a full-factorial design exercises all combinations of discrete values defined for each model parameter. Herein, the discrete values are called "levels;" they are defined as equally spaced increments between the lower and upper bounds of each parameter. Fig. 9 illustrates a notional full-factorial design of spring stiffness coefficients (k_{nn}; k_{ss}; k_{tt}) of Table 8. Three levels are defined for the first two parameters (k_{nn}; k_{ss}) and five levels are defined for the third parameter k_{tt}. Simulating all combinations of the full-factorial design would require a total of $3 \times 3 \times 5 = 45$ runs of the FE model.

Fig. 10 illustrates the first four resonant modes predicted by the tied node FE model. Results for the contact stiffness representation are similar (not shown). These predictions can be compared to the experimentally identified mode shapes of Fig. 4, and it is observed that the deflections are similar. Ensuring correct pairing is especially important when parameters of the models are varied, and the possibility of mode "swapping" (for example, the second mode appears at the third position and vice-versa) cannot be discounted.

While the FE models and related experimental data are not publicly available, readers interested accessing them are encouraged to contact the authors. It might be possible to share these datasets based on a case-by-case agreement for collaboration and explanation of intended usage.

Table 8
Parameterization of the two finite element models.

Modeling strategy	Unknown parameters
Contact stiffness representation	Spring stiffness coefficients (k_{nn}; k_{ss}; k_{tt})
Tied node representation	Radius-of-influence (r)

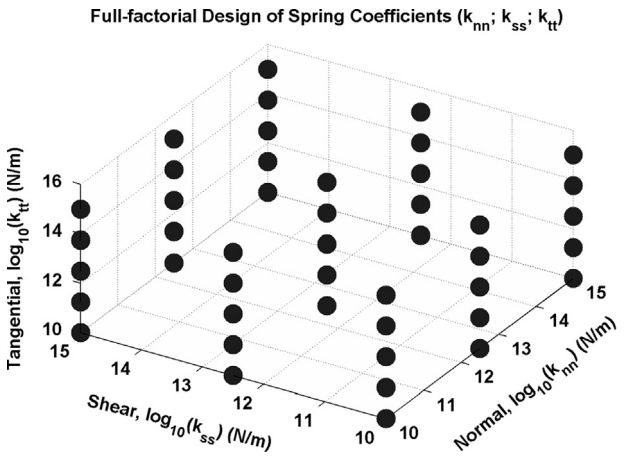

Fig. 9. Full-factorial design of experiments for three spring coefficients (k_{nn}; k_{ss}; k_{tt}).

Fig. 10. First four resonant mode shapes predicted by the tied node FE model.

4.2. Quantification of numerical uncertainty for the finite element simulations

Mesh refinement studies are carried out for various subassemblies of the FE model in order to quantify the numerical uncertainty, due to truncation error, of resonant frequency predictions as a function of grid size. Here, "truncation" refers to the approximation generated when the continuous governing equations are discretized onto a 3-D mesh with elements of height (Δx), width (Δy), and length (Δz). Meshes with varying sizes are created and evaluated. The predictions of resonant frequencies are analyzed to quantify the truncation error produced by each mesh size. In short, the analysis compares predictions obtained from successively refined meshes to estimate, first, the rate-of-convergence of the numerical solver and, second, upper bounds of truncation error. Further details of this mesh refinement procedure can be found in Ref. [7]. The magnitude of truncation error is used to determine the appropriately sized mesh that should be implemented in the FE model. Predictions of the first natural frequency are obtained by analyzing the same model with five mesh resolutions, using 1, 2, 3, 4, and 8 elements through the thickness of the top beam. The mesh sizes chosen for all elements have an aspect ratio of near one, whereby the height, width, and length of each element are nearly constant (i.e. $\Delta x \approx \Delta y \approx \Delta z$). The size of each mesh is dictated by the number of elements through the smallest thickness in the subassembly.

A first mesh refinement study is applied to a straight beam with rectangular cross-section, 152.4 mm long, 25.4 mm wide, and 9.5 mm thick, whereby a closed-form solution is available for the first natural frequency [19]. When the exact solution is known, truncation error is simply the difference between the FE prediction and the exact solution. A second refinement study is applied to the 90-degree bracket connection of the portal frame. Since no closed-form solution is available for this geometry, the technique of Richardson's extrapolation presented in Ref. [20] is used to estimate the value of the first resonant frequency as the mesh size converges to zero. Upper bounds of truncation error are then derived from differences between this extrapolation and FE predictions obtained from successively refined meshes [7]. It is emphasized that truncation is exclusively a property of the FE discretization selected to perform a calculation and, therefore, comparison with physical measurements is not relevant at this stage.

Discretizing the structural components with three elements through the thickness provides a truncation error of 5.64% for the straight beam problem and 2.34% for the 90-degree bracket problem. Using only two through-thickness elements increases the truncation error to 13.27% for the straight beam problem, which is deemed too large. Computing, on the other hand, with four through-thickness elements, while requesting a near-unity aspect ratio everywhere, greatly increases the time-to-solution. With these considerations, a discretization with three elements through the thickness is selected for the portal frame [14].

The resulting, nominal FE model features a total of 105,400 nodes and 75,534 finite elements. A modal analysis performed to extract the low-frequency mode shapes is solved in ≈ 1 min on a typical PC workstation, which is fast enough to perform a few hundred runs for the parameter studies presented next. This discretization, with three through-thickness elements (top beam, side columns, brackets, and base plate), is identical for all runs performed.

4.3. Parameter study of the contact stiffness representation

Spring coefficients of the contact stiffness representation are investigated next. The first step is to decide bounds within which these values must be varied. It is observed that, for values lower than 10^{+10} N/m, the order of the modes changes. This is an indication that the contact surface condition deviates from the experimental condition and, therefore, the spring coefficients used in the FE model are not appropriate. On the other hand, the resonant frequencies asymptote to constant values when the spring coefficients exceed 10^{+15} N/m. It indicates that the jointed connection is essentially "rigid" and further increasing the spring stiffness values has no effect. These two observations set the lower and upper bounds of stiffness coefficients to the range [10^{+10} N/m; 10^{+15} N/m]. The parameter study is pursued using these lower and upper bounds.

To keep the study to a manageable size, all of the bolts of the bracket-to-vertical column and bracket-to-top beam connections are grouped together and assigned the same stiffness values in the normal, shear and tangential directions. These coefficients are denoted by k_{nn} (normal), k_{ss} (shear) and k_{tt} (tangential). Similarly, the 10–24 socket cap screws of the bracket-to-base plate connections are grouped together and assigned the same stiffness values k_{nn}, k_{ss} and k_{tt}. This parameterization of the model gives six spring coefficients where each is varied within the lower and upper bounds [10^{+10} N/m; 10^{+15} N/m].

A two-level, full-factorial design-of-computer-experiments is defined to propagate the bounds of spring stiffness values through the model. Predictions are used to observe the effect on the first four resonant frequencies of changing one spring at a time. This analysis is similar to the main-effect analysis applied to measured resonant frequencies in Section 3.4.

The ANOVA results of Fig. 11 clearly indicate that one of the bolt shear parameters ("bolt k_{ss}") and the base plate normal stiffness ("base k_{nn}") are the two most influential parameters for the four resonant frequencies. They must be considered to quantify the prediction uncertainty. Observing that the bolt shear stiffness coefficient is one of the most influential parameters of the FE model matches the intuition gained from experimental campaigns, where observations suggest that most of the target modes are sensitive to shearing effects of the jointed connections. The ANOVA also indicates that the other four stiffness coefficients can be eliminated from further consideration since varying them from the lower to upper bounds does not significantly change the frequency predictions. These four parameters are kept constant and equal to mid-range values ($3.16 \times 10^{+12}$ N/m, mid-point on a $\log_{10}$-scale).

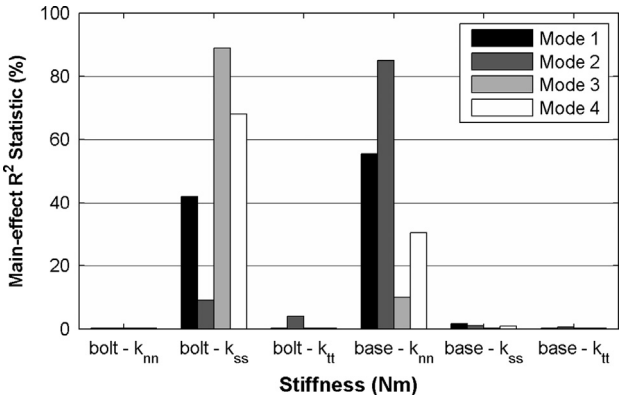

Fig. 11. Main-effect ANOVA of predicted frequencies (contact stiffness FE model).

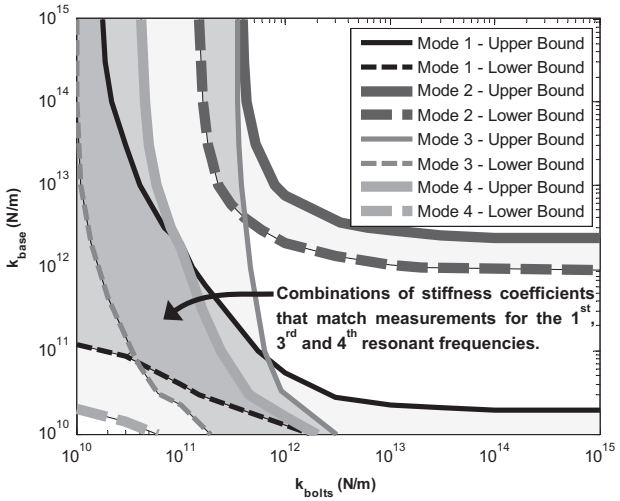

Fig. 12. Filled contours indicating where predictions are within the measurement variability for the 4.52 Nm torque case.

Having eliminated four of the six spring coefficients, an eleven-level, full-factorial design is analyzed next, where all of the bolt coefficients are grouped together and, likewise, all of the base plate coefficients are grouped together. The two groups are denoted by k_{Bolt} and k_{Base} that correspond, respectively, to the symbols "bolt k_{ss}" and "base k_{nn}" used previously. Because it features more than two levels per parameter, this second design can capture potential nonlinear effects of varying one of the stiffness coefficients, or two coefficients simultaneously. The design results in an additional $11^2=121$ runs of the FE model.

The results of this study are used to observe the combinations of spring coefficients (k_{Bolt}; k_{Base}) that provide frequency predictions that "match" the measurements. "Matching," here, is not an attempt to reproduce the measured values as best as possible; our criterion is, instead, to produce predictions that reside within the lower and upper bounds estimated from the experimental campaigns. This is achieved by determining the pairs of coefficients that give a particular frequency, then plotting the iso-frequency values that correspond to the lower and upper bounds of measurements (see Table 7). Two contours are obtained from this process, corresponding to the overall range of experimental observations. Fig. 12 illustrates results of the process, repeated for the first four modes.

Regions of Fig. 12 shaded in light gray indicate combinations of spring coefficients (k_{Bolt}; k_{Base}) that comply with the criterion *"predict a frequency within the experimental variability"* for a given frequency and torque level. Darker shades of gray highlight regions where multiple selection criteria overlap.

It can be observed that a common overlap can be found for the first, third and fourth resonant frequencies. This is true for all torque levels. No pair of stiffness coefficients (k_{Bolt}; k_{Base}) is found, however, that provides a common overlap for the second mode (torsional mode). The inability to match all four frequencies simultaneously suggests that the FE model parameterization is not appropriate to capture torsional effects. Varying the stiffness coefficients independently, instead of grouping them together, has not been attempted due to the time constraint of a study limited to ten weeks. In addition, ANOVA results from the experimental testing suggest that the level of bolt torque is most influential. The fact that the method and sequence of bolt tightening are of lesser influence experimentally suggests that all of the bolts maintain

a similar fit, which makes it reasonable to group all bolts together. Not being able to capture well the second mode might also suggest a fundamental flaw with the contact stiffness representation.

4.4. Parameter study of the tied node representation

The parameter study of the tied node representation is similar to the previous one, except that it involves a single parameter: the radius-of-influence of the bolted joint. Here, the radius is incrementally increased from 5 mm to 30 mm. The lower bound of 5 mm is selected because it defines an area smaller than the surface area of the bolt head/nut. The surfaces defined for $5\text{ mm} \leq r \leq 25\text{ mm}$ provide a circular contact. The upper bound of 30 mm defines a circle that falls partially outside the face of the bracket, whose dimension is 63.5 mm by 50.8 mm. The tied condition is applied only to nodes of the bracket face that overlap with those of the surface-of-influence. Since there is only one parameter to consider, the study is simpler than previously. The goal is nevertheless similar: search for radius-of-influence values that define FE models whose predictions reside within the range of measured frequencies assessed experimentally.

Fig. 13 displays how the first four resonant frequencies change when the radius-of-influence varies within the interval [5 mm; 30 mm]. All radii of bolt connections are varied in a similar manner. Due to computational resource and time constraints, the scenario where each bolted connection would define its own radius-of-influence is not analyzed. For comparison, measured frequency ranges obtained with the 9.04-Nm torque are indicated with thicker solid lines. Only the 9.04-Nm torque case is illustrated in Fig. 13 because the other cases give similar observations.

As expected, the resonant frequencies increase as the radius-of-influence increases, causing the joints to behave more rigidly. Frequencies of the first, second and fourth modes experience significant changes in value with the increase in contact radius. Frequencies of the third mode (out-of-phase bending mode) do not experience as much change. This trend is consistent with the results of physical testing where it is observed that the third-mode resonant frequency exhibits the smallest variance at all bolt torque levels (see Table 7).

Fig. 13 suggests that a non-zero intersection of radii-of-influence can be found such that the corresponding FE models predict their first four resonant frequencies within the measurement ranges determined experimentally. These predictions correspond to tied node radii of the FE models between 25.8 mm and 26.5 mm. The facts that, first, a range of radii-of-influence that meet our selection criteria is found and, second, the model reproduces the experimental trends, indicate that simplifying the parameterization to a single radius-of-influence suffices to establish positive test-analysis correlation. Therefore, more elaborate studies, where several radii are defined and varied independently, are not pursued.

5. Test-analysis correlation and assessment of bounding predictions

The last part discusses the test-analysis correlation obtained from the measurement ranges assessed in Section 3 and prediction bounds of Section 4. The ranges of resonant frequencies obtained experimentally by varying the bolt torque, method of bolt tightening and sequence in which the bolts are tightened are compared to the lower and upper bounds of predictions obtained from parameter studies of the two "bounding-case" joint modeling strategies.

It is emphasized that our test-analysis comparison examines the "spread" of frequency values obtained with different model forms. This approach is different from a calibration study where, first, the model form is "frozen," and, second, parameters are optimized such that predictions reproduce the measurements as closely as possible. It would be possible to calibrate one FE model or another, however, our purpose is to quantify model-form uncertainty by evaluating the effect of implementing different representations of the structural joints.

Having said so, the calibration of model parameters is implicitly illustrated in Figs. 12 and 13. As indicated by the shaded regions of Fig. 12 (contact stiffness representation), different combinations of spring coefficients (k_{Bolt}; k_{Base}) provide "acceptable" predictions, that is, values located within the experimental ranges. Similarly in Fig. 13 for the tied node

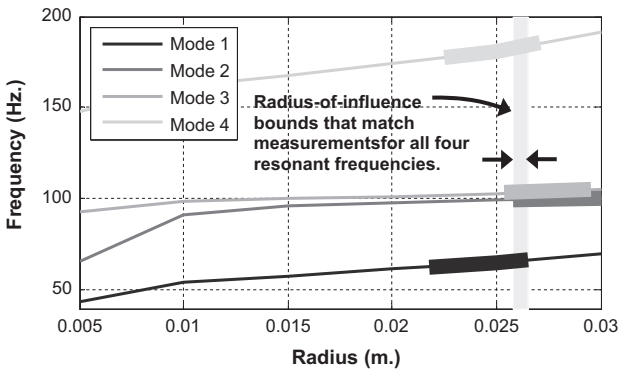

Fig. 13. Parameter study of the radius-of-influence for the 9.04 Nm torque case.

representation, different radii-of-influence lead to acceptable predictions. Of course, some of these predictions better reproduce the measurements than others. These results indicate the non-uniqueness of calibrated solutions.

Test-analysis correlation is summarized in Table 9 for the first four frequencies. The table lists the lower bounds, upper bounds and overall ranges of resonant frequencies. Ranges given in column 3 for the measured frequencies are identical to those of Table 7; they encompass the three bolt torque levels tested experimentally. For the FE predictions, the bounds reported are those obtained by varying parameters of the model over their entire ranges.

Not captured in Table 9 is the fact that the contact stiffness representation is unable to predict all four frequencies with the same pair of parameters (k_{Bolt}; k_{Base}). Table 9 shows that the prediction bounds obtained from this model are able to fully "envelope" experimental measurements of the first, third and fourth modes. This is not the case for the second mode where the upper measurement bound is higher than the higher prediction bound. It suggests that the contact stiffness representation is incapable of capturing the torsional movement of the second mode, which is likely due to the fact that the rigidity/compliance conditions of the FE model are applied to the entire surfaces of the bracket-to-beam connections.

In contrast, the tied node representation is able to simultaneously capture all four frequencies for a range of radius-of-influence values. Table 9 shows that the model consistently provides lower bounds that are lower than those measured experimentally. This trend can be explained by the definition of the parametric study, which pursued radii ranging from 5 mm to 30 mm. The actual bolts of the portal frame are 12.7 mm in diameter, and the face of brackets measures 63.5 mm by 50.8 mm. Table 9 also shows that the tied node representation is unable to predict resonant frequencies that are higher than the upper bounds of experimental measurements. As a result, predictions of this model do not "envelope" the measurements. This observation contrasts with results of the contact stiffness representation, which successfully encompasses measurements for three of the four vibration modes. We have verified that resonant frequencies predicted with large spring coefficients, that is, k_{Bolt}, $k_{\text{Base}} \geq 10^{+15}$ N/m, converge to values obtained when rigid connections are imposed over the entire contact surfaces of brackets. It suggests that restricting the tied node condition to a circular radius does not define a rigid-enough compliance that reproduces the experimental conditions. Allowing forces to be transmitted across the entire surface of the bracket-to-beam connection, as is done with a contact stiffness representation, is more appropriate to simulate high torque levels for the first, third and fourth vibration modes.

Table 10 gives a summary of various sources of uncertainty in the analysis of the portal frame. Column 2 lists the measurement ranges of resonant frequencies reported in Table 7. Columns 3–4 and 5–6 give the discretization and parametric ranges for the contact stiffness and tied node models, respectively. These prediction ranges are defined as differences between the upper and lower bounds estimated from our sensitivity analyses and parametric studies. Differences between averaged frequency predictions of the two representations are listed in the last column. This simple metric quantifies model-form uncertainty, that is, the first-order effect on predictions of changing from the contact stiffness model to the tied node model.

The first observation from Table 10 is that, except for the second (torsional) mode, the model-form uncertainty (column 7) is comparable to truncation error (columns 3, 5). It would be difficult to argue that one type of uncertainty is more significant than the other one. To achieve better prediction accuracy, one would need to simultaneously increase the level of resolution with which a calculation is performed, and implement a higher-fidelity representation of the joint. The close agreement between the two representations for the second frequency reflects the fact that neither model captures well the torsional deformation, especially at high bolt torque. The second observation from Table 10 is that, in all cases, varying model parameters produces wider prediction bounds than either truncation error or model-form uncertainty. We conclude that, for

Table 9
Ranges of measured and predicted resonant frequencies of the first four modes.

Resonant mode	Measurements		Contact stiffness model		Tied node model	
	Bounds (Hz)	Range (Hz)	Bounds (Hz)	Range (Hz)	Bounds (Hz)	Range (Hz)
1	58.8-to-71.6	12.8	53.8-to-73.1	19.3	43.5-to-70.4	26.9
2	97.5-to-103.0	5.5	65.8-to-101.2	35.4	65.5-to-100.5	35.0
3	102.0-to-106.0	4.0	100.4-to-106.2	5.8	93.2-to-105.3	12.1
4	170.0-to-193.0	23.0	168.5-to-198.3	29.8	148.0-to-191.7	43.7

Table 10
Experimental, truncation, parameter and model-to-model uncertainties.

Resonant mode	Measurement range (Hz)	Contact stiffness model		Tied node model		Model-to-model difference (Hz)
		Truncation (Hz)	Range (Hz)	Truncation (Hz)	Range (Hz)	
1	12.8	3.8	19.3	3.4	26.9	6.5
2	5.5	5.0	35.4	5.0	35.0	0.5
3	4.0	6.2	5.8	6.0	12.1	4.0
4	23.0	11.0	29.8	10.2	43.7	13.6

this particular application, model-form is not the main driver of prediction uncertainty. Calibration or small-scale experiments that focus on the joint dynamics would be needed to further reduce the unknown ranges of model parameters such that the numerical predictions become more consistent with the experimental variability.

In summary, we are left with a modeling dilemma. The contact stiffness representation, that defines fictitious stiffness conditions between coincident nodes of the entire surface, is able to "envelope" the frequency measurements; it fails, however, to capture the torsion mode well. The tied node representation defines a physically more realistic description of the contact; it does not, however, provide enough rigidity especially when combined with high torque levels.

6. Conclusion

This paper discusses the experimental and numerical analyses of the first four vibration modes of a nominally symmetric one-story portal frame structure. The experimental campaigns quantify variability due to changing the bolt torque, method by which the bolts are tightened, and sequence in which the bolts are tightened. The results support the idea that, as the torque is increased, the contact condition becomes more rigid, which causes the measured resonant frequencies to increase. Through analysis-of-variance, it is found that the bolt torque is the most influential factor for the second, third and fourth resonant frequencies. The first-mode frequency, that involves a shearing deformation, is equally influenced by the bolt torque and sequence in which the bolts are tightened. These findings drive the definition of modeling rules to represent the bracket-to-beam connections with two finite element models.

Two competing finite element models of the portal frame are developed using solid elements with differing assumptions to represent the joints: (i) contact stiffness coefficients and (ii) tied nodes. Mesh refinement is executed to select an appropriate discretization. The contact stiffness representation defines fictitious springs between coincident nodes of the contact surfaces. All nodes of contact surfaces are connected in this manner. The tied node representation defines a tied constraint that does not permit relative displacement between coincident nodes located within a radius-of-influence.

Parameter studies of the two competing models are pursued to assess the bounds of frequency predictions. The third resonant frequency of the out-of-phase bending mode is predicted by both models with the least variability. This is consistent with the experimental variability assessed from measurements. It is explained by the fact that this bending mode is more reliant on bolt properties than bolt torque level. When parameters of the contact stiffness representation are varied, predictions are able to "envelope" the experimental variability for the first, third and fourth resonant frequencies. This is not the case, however, for the second frequency of the torsion deformation mode. In comparison, the tied node representation gives frequency predictions that are consistent with the experimental variability for the four resonant modes considered. The tied node model is unable, however, to represent the upper range of experimental variability for any of the frequencies. In particular, neither joint modeling rule captures well the torsional mode at high bolt torque.

Future work could include the development of models that better capture the torsional effects. One suggestion is to add point masses to the face of the top beam where bolt heads are located. Mass loading might affect the torsional deformation in ways that are different than varying the bolt torque level. Another suggestion is to parameterize the FE representation of joints with rotational springs in addition to the torsional springs considered in this work. Other model forms, such as discretizing the bolts with three-dimensional solid elements, can also be pursued. Herein, test-analysis correlation of the numerical model to experiments considered only the resonant frequencies of the first four mode shapes. Future work could consider mode shape vectors, entire frequency response functions, entire time history responses, and other features that quantify performance, for assessing the correlation of numerical predictions to test data.

This study demonstrates the benefits of implementing simplified modeling rules, however, only when the effects of these assumptions are studied and understood. This is what we propose through parameter studies and test-analysis correlation assessments of different model forms. We argue that this strategy yields a more thorough quantification of model-form uncertainty, instead of only relying on calibration to improve the accuracy of predictions.

Acknowledgments

This work is performed under the auspices of the Los Alamos National Laboratory (LANL) as part of the Los Alamos Dynamics Summer School (LADSS). The authors are grateful to Dr. Charles Farrar, The Engineering Institute, for organizing the LADSS. The authors also wish to express their gratitude to Dr. Peter Avitabile, University of Massachusetts Lowell, for guidance in the experimental testing. The companies Simulia and Vibrant Technology, Inc., graciously contributed Abaqus™ and ME'Scope software licenses to the LADSS, without which this work would not have been possible. LANL is operated by the Los Alamos National Security, L.L.C., for the National Nuclear Security Administration of the U.S. Department of Energy under Contract DE-AC52-06NA25396.

References

[1] J.R. Alfaro, I. Arana, S. Arazuri, C. Jarén, Assessing the safety provided by SAE J2194 standard and code 4 standard code for testing ROPS, using finite element analysis, Biosyst. Eng. 105 (2010) 189–197.

[2] ASCE, Minimum Design Loads for Buildings and Other Structures, American Society of Civil Engineers, Reston, VA, 1998.

[3] SAE J2940, Use of Model Verification and Validation in Product Reliability and Confidence Assessments, Ground Vehicle Reliability Committee, October 2011.
[4] Veritas Det Norske, Design and Manufacture of Wind Turbine Blades, Offshore and Onshore Wind Turbines, October 2010.
[5] G. Freebury, W. Musial, Determining Equivalent Damage Loading for Full-scale Wind Turbine Blade Fatigue Tests, 19th ASME Wind Energy Symposium, Reno, Nevada, 2000.
[6] C.J. Freitas, The issue of numerical uncertainty, Appl. Math. Model. 26 (2002) 237–248.
[7] M.G. Mollineaux, K.L. Van Buren, F.M. Hemez, S. Atamturktur, Simulating the dynamics of wind turbine blades: part I, model development and verification, Wind Energy 16 (2013) 694–710.
[8] D. Veldkamp, A probabilistic evaluation of wind turbine fatigue design rules, Wind Energy 11 (2008) 655–672.
[9] G.E. Wilson, B.E. Boyack, The role of the PIRT process in experiments, code development and code applications associated with reactor safety analysis, Nucl. Eng. Des. 186 (1998) 23–37.
[10] C. Chatfield, Model uncertainty, data mining, and statistical inference, J. R. Stat. Soc. Ser. A (Stat. Soc.) 158 (1995) 419–466.
[11] D.J. Ewins, D.J. Inman (Eds.), Structural Dynamics @2000: Current Status and Future Directions, Baldock Research Studies Press, 2000.
[12] D.J. Segalman, D.L. Gregory, M.J. Starr, B.R. Resor, M.D. Jew, J.P. Lauffer, N.M. Ames, Handbook on Dynamics of Jointed Structures, Technical Report SAND2009-4164, Sandia National Laboratories, Albuquerque, New Mexico, July 2009.
[13] F.M. Hemez, P.J. Cornwell, P. Avitabile, Validation of Finite Element Predictions of the Dynamic Response of a Frame Structure, in: Proceedings of the 26th SEM International Modal Analysis Conference, Orlando, Florida, February 4–7, 2008.
[14] L.M. Gonzales, T.M. Hall, K.L. Van Buren, S.R. Anton, F.M. Hemez, Quantification of Prediction Bounds Caused by Model Form Uncertainty, Technical Report LA-UR-13-27561, Los Alamos National Laboratory, Los Alamos, New Mexico, September 2013.
[15] Abaqus/CAE User's Manual (6.12), ABAQUS, Inc., 2012.
[16] M. Palmonella, M.I. Friswell, J.E. Mottershead, A.W. Lees, Guidelines for the implementation of the cweld and acm2 spot weld models in structural dynamics, Finite Elem. Anal. Des. 41 (No. 2) (2004) 193–210.
[17] D.J. Segalman, A four-parameter Iwan model for lap-type joints, ASME J. Appl. Mech. 72 (2005) 752–760.
[18] J. Hegenderfer, S. Atamturktur, Prioritization of code development efforts in partitioned analysis, Comput. Aided Civil Infrastruct. Eng. 28 (4) (2013) 289.
[19] D.R. Blevins, Formulas for National Frequency and Mode Shape, Krieger Publishing Company, Malabar, Florida, 1993.
[20] P.J. Roache, Verification and Validation in Computational Science and Engineering, Hermosa Publishers, Albuquerque, New Mexico, 1998.